Title: The January 2022 eruption of Hunga Tonga-Hunga Ha'apai volcano reached the mesosphere

Authors: Simon R Proud[1,2]*, Andrew T Prata[2], Simeon Schmauß[3]

Affiliations:

[1]National Centre for Earth Observation, RAL Space, STFC Rutherford Appleton Laboratory, Harwell, OX11

[2]Atmospheric, Oceanic and Planetary Physics, University of Oxford, Parks Road, Oxford, OX1 3PU

[3]Munich University of Applied Sciences, Lothstr. 34, 80335 Munich, Germany

*Corresponding author. Email: simon.proud@stfc.ac.uk

Abstract: Explosive volcanic eruptions can loft ash, gases and water into the stratosphere, which affects both human activities and the climate. Using geostationary satellite images of the January 2022 Hunga-Tonga volcano eruption we find that the volcanic cloud produced by this volcano reached an altitude of 57km at its highest extent. This places the cloud in the lower mesosphere and provides the first observational evidence of a volcanic eruption injecting material through the stratosphere and directly into the mesosphere. We then discuss potential implications of this injection and suggest that the altitude reached by plumes from previous eruptions, such as Pinatubo in 1991, are very likely to be underestimated.

One-Sentence Summary: Large volcanic eruptions often reach the stratosphere, but here we show evidence that the January 2022 eruption of Hunga-Tonga reached beyond the stratosphere and into the mesosphere.

Main Text: Large explosive volcanic eruptions are significant as they can impact climate *(1)*, disrupt aviation *(2)* and pose a numerous hazards to communities living nearby active volcanoes *(3, 4)*. The degree to which explosive volcanic eruptions affect climate is largely dependent on the volcano's latitude, the plume height, and the amount of SO2 gas that is released *(5)*. When a significant amount of SO2 is released into the stratosphere it converts to sulphate aerosols that can, in the most extreme cases, persist for several years *(6)* and when injected at low latitudes the aerosol disperses into both hemispheres *(1, 7)*. The persistent aerosol veil that is produced impacts climate due to the reflection of incoming visible radiation and absorption of near-infrared radiation *(8)*, that results in a cooling of the troposphere *(9)* and heating of the stratosphere *(10)*. Within the satellite era, there are numerous examples of volcanic plumes reaching the upper-tropopause lower-stratosphere (UTLS) *(11,12)*; however, few have been observed to reach higher than 30 km and impact the climate *(13)*. Notable examples that have been observed and quantified using satellite observations include Mt Pinatubo (Philippines) in 1991 that injected ~20 Tg of SO2 *(14)* and reached 40 km at its highest point *(15)* and El Chich´on that released ~7.5 Tg of SO2 into the atmosphere *(16)*, reaching 31 km *(17)*. Based on the satellite data record, in general, individual explosive volcanic eruptions are not expected to have a measurable climate impact unless >1 Tg SO2 is released into the stratosphere *(13)*.

The Hunga Tonga-Hunga Haapai volcano (20.536°S, 175.382°W) is an underwater caldera volcano located approximately 70 km North-northwest of Tonga's capital, Nukualofa. Recent Surtseyan-style eruptive activity was observed in 2009, 2014-15 and from 20 December 2021 *(18)*. In the lead up to the 15 January 2022 eruption, described below, a large hreatomagmatic eruption, similar to the December 2019 eruption of Anak Krakatau, Indonesia *(19)*, was observed on 13 January in geostationary satellite data. The volcanological setting of Hunga Tonga-Hunga Haapai is very different compared to the Pinatubo and El Chich´on volcanoes due to the abundance of seawater available for magma interaction. Initial estimates of the total mass of SO2 released by the 15 January eruption from hyperspectral sounders and ultraviolet instruments was 0.2-0.4 Tg SO2 *(20)*. This amount of SO2 is low given the magnitude of this eruption and suggests that large amounts of SO2 may have been scavenged through wet deposition *(19, 21)*.

On 15th January 2022 at approximately 4am UTC (5pm local time) the Hunga-Tonga volcano violently erupted, producing the large volcanic cloud, shown in Figure 1. A second, smaller, eruption occurred at 8am UTC with no further large eruptions occurring thereafter. This eruption was one of the most powerful in recent years, triggering a tsunami that was felt across the Pacific and atmospheric waves that circled the Earth multiple times, which were seen as fluctuations in global pressure sensor readings for several days. The volcano's location is well-covered by satellite sensors, with three geostationary weather satellite platforms providing imagery of the area at visible and infrared wavelengths every ten minutes, summarized in supplementary Table 1, and at approximately 07:05 UTC the National Oceanic and Atmospheric Administration (NOAA) enabled a fast-scanning mesoscale sector over the volcano, producing imagery every minute.

Typically, the altitude of a volcanic plume is estimated from its cloud top temperature measured by satellite compared to a vertical profile of temperature from radiosonde measurements or weather model output such as that produced by the European Centre for Medium-Range Weather Forecasts (ECMWF) *(22)*. This technique makes use the relationship of decreasing atmospheric temperature - and hence cloud temperature for a cloud in thermodynamic equilibrium with its surroundings - with altitude in the troposphere *(23)*. However, for large volcanic eruptions the cloud penetrates the tropopause and enters the stratosphere where temperature increases with

altitude, thus rendering temperature-based techniques inaccurate: In such cases the plume in the stratosphere will initially be cooler than the ambient air but will warm as the plume enters thermodynamic equilibrium with its surroundings, which presents several possible altitude solutions for a single cloud temperature. This is further complicated as the eruption itself is likely to affect local vertical temperature profiles. In this report, we make use of the multiple satellite sensors that viewed the eruption from very different viewing geometries to compute plume altitude based on the parallax effect, which does not suffer from the limitations described above, and find that the Hunga-Tonga eruption not only penetrated the stratosphere but reached the lower mesosphere.

When a satellite views a high-altitude cloud, the cloud location within the satellite image will be incorrect due to a parallax shift whose magnitude depends on the viewing angle between satellite and cloud and upon the cloud altitude. If two or more satellites view a cloud from differing locations, then its actual position and altitude are found by iteratively adjusting estimated cloud altitude to minimize the difference in parallax corrected position between satellites *(24)*. We have previously used this approach to successfully estimate the altitude and trajectory of the Chelyabinsk Meteor *(25)*, demonstrating that the technique is appropriate for high altitude clouds. Here, we apply the approach to a series of manually selected cloud positions observed by Himawari-8 and GEO-KOMPSAT-2A (GK-2A) to the West of the Eruption and GOES-17 to the East across images taken between 04:16 UTC and 06:36 UTC, after which the sun set. In addition, we perform a more detailed analysis of the 04:36 UTC imagery from Himawari-8 and GK-2A to map variations in altitude across the plume, which is shown in Figure 2. Because these methods rely on manual point selection and analysis, they cannot map altitude across the whole plume. To gain a broad perspective of plume altitude we therefore also applied a stereoscopic vision tool to estimate altitude, which is less accurate but can provide spatial information, and the standard temperature-based retrieval described above. The results of all three techniques are shown in Fig 3. Further information on the methods used here, including tables of parallax-retrieved altitudes, are given in the supplementary materials.

Altitude retrievals from the early phase of the eruption show a rapidly ascending cloud layer, reaching 25km approximately 15 minutes after the eruption begun and 40km, in the upper stratosphere, after 25 minutes. By 04:36, half an hour after the eruption began, a dome of cloud, approximately 90km in diameter, is visible that extends from 34km up to 57km altitude (approx. 0.3hPa in the ECMWF analysis), which is 13km above the stratopause (1.5hPa) – well within the mesosphere. We estimate the uncertainty on this altitude to be less than 1.5km. Surrounding this dome is a donut-shaped structure with altitudes peaking at 41km (2.2hPa) and a secondary layer just above the ECMWF tropopause at 17.5km (91hPa). A schematic of the eruption at this point is shown in Fig 4. Ten minutes later, the dome collapsed to leave the expanding donut cloud, although haziness visible in the central region above the volcano indicates that high altitude aerosol such as sulphates or ash is likely to be present. This haze is too optically thin, however, to support altitude retrieval. By 04:56 UTC the eruption produced a new vertical column of cloud stretching from the surface to the mesosphere, including two tendrils that reach 58km (0.28hPa). These tendrils cast a shadow onto the main volcanic umbrella, now at 35km altitude, and calculation tendril altitude from the shadow length gives an altitude of 57.5km, closely matching the parallax-derived altitude. Thereafter, as shown in Fig 3, plume altitude decreases and no further mesospheric intrusions were detected. Analysis of the infrared imagery shows two plumes over the next twelve hours: One, moving South-West in the prevailing winds at 30-35km altitude and one moving East at the tropopause.

The influence of volcanoes on the mesosphere is unclear. Previous eruptions into the stratosphere have indirectly affected the mesosphere through the upward ascent transport of volcanic aerosols after an eruption *(26)*, although the chemical processes acting on mesospheric volcanic aerosols are the subject of debate *(27)*. Vertical propagation of gravity waves from volcanoes can affect the mesospheric temperature *(28)* while the aerosols and water vapor injected to high altitude by the Krakatoa eruption may have been responsible for subsequent apparent increases in mesospheric cloud. However, there is no agreement as some volcanic eruptions but not others are associated with mesospheric cloud increases *(29)*. Our observations of the Hunga-Tonga plume provide the first direct evidence that volcanic eruptions can inject material into the mesosphere and will enable more detailed analysis of mesospheric chemistry and transport. However, our work also raises questions - what mechanisms contributed to this eruption reaching such high altitude and yet appears to have released comparatively little SO2? What is the hazy substance visible atop the highest clouds and how long will it persist in the mesosphere? In addition, we show that the mesospheric altitudes achieved by this plume were only visible in satellite images taken at two times (04:30 and 04:50 UTC), highlighting the importance of frequent - every ten minutes in this case - satellite observations. Previous eruptions, such as Pinatubo, were observed much less frequently by satellite, making it very likely that the time of peak altitude associated with their volcanic plumes was not observed and that we are likely to be underestimating plume altitude by a significant amount.

References and Notes

1. Robock, Volcanic eruptions and climate 38, 191–219.

2. T. J. Casadevall, Volcanic ash and aviation safety: proceedings of the first international symposium on volcanic ash and aviation safety, no. 2047 (US Government Printing Office, 1994).

3. S. C. Loughlin, et al., Global volcanic hazards and risk (Cambridge University Press).

4. T. M. Wilson, S. Jenkins, C. Stewart, Volcanic Hazards, Risks and Disasters (Elsevier, 2015), pp. 47–86.

5. C. Schnetzler, G. Bluth, A. Krueger, L. Walter, A proposed volcanic sulfur dioxide index (vsi), Journal of Geophysical Research: Solid Earth 102, 20087–20091 (1997).

6. S. Kremser, et al., Stratospheric aerosol-observations, processes, and impact on climate: Stratospheric aerosol 54, 278–335.

7. J. Hansen, A. Lacis, R. Ruedy, M. Sato, Potential climate impact of mount pinatubo eruption, Geophysical Research Letters 19, 215–218 (1992).

8. G. L. Stenchikov, et al., Radiative forcing from the 1991 mount pinatubo volcanic eruption 103, 13837–13857.

9. E. G. Dutton, J. R. Christy, Solar radiative forcing at selected locations and evidence for global lower tropospheric cooling following the eruptions of el chich´on and pinatubo 19, 2313–2316.

10. K. Labitzke, M. P. McCormick, Stratospheric temperature increases due to Pinatubo aerosols 19, 207–210.

11. G. L. Stenchikov, et al., Radiative forcing from the 1991 mount pinatubo volcanic eruption, Journal of Geophysical Research: Atmospheres 103, 13837–13857 (1998).

12. A. Bernard, W. I. Rose, The injection of sulfuric acid aerosols in the stratosphere by the el chich´on volcano and its related hazards to the international air traffic, Natural Hazards 3, 59–67 (1990).

13. S. Carn, L. Clarisse, A. Prata, Multi-decadal satellite measurements of global volcanic degassing 311, 99–134.

14. S. Guo, G. J. Bluth, W. I. Rose, I. M. Watson, A. Prata, Re-evaluation of so2 release of the 15 June 1991 Pinatubo eruption using ultraviolet and infrared satellite sensors, Geochemistry, Geophysics, Geosystems (2004)

15. R. E. Holasek, S. Self, A. W. Woods, Satellite observations and interpretation of the 1991 mount pinatubo eruption plumes 101, 27635–27655.

16. A. Krueger, N. Krotkov, S. Carn, El chichon: The genesis of volcanic sulfur dioxide monitoring from space 175, 408–414.

17. M. Matson, The 1982 el chich´on volcano eruptions — a satellite perspective 23, 1–10.

18. M. Brenna, et al., Post-caldera volcanism reveals shallow priming of an intra-ocean arc andesitic caldera: Hunga volcano, Tonga, SW pacific.

19. A. T. Prata, et al., Anak krakatau triggers volcanic freezer in the upper troposphere

20. S. K. e. Sennert, Report on hunga tonga-hunga ha'apai (tonga).

21. W. I. Rose, et al., Ice in the 1994 rabaul eruption cloud: implications for volcano hazard and atmospheric effects 375, 477–479.

22. R. G. Owens, T. Hewson, Ecmwf forecast user guide (2018).

23. M. Stengel, et al., Cloud property datasets retrieved from avhrr, modis, aatsr and meris in the framework of the cloud cci project, earth syst. sci. data, 9, 881–904 (2017).

24. L. Merucci, K. Zakˇsek, E. Carboni, S. Corradini, Stereoscopic estimation of volcanic ash cloud-top height from two geostationary satellites, Remote Sensing 8, 206 (2016).

25. S. Proud, Reconstructing the orbit of the chelyabinsk meteor using satellite observations, Geophysical research letters 40, 3351–3355 (2013).

26. M. J. Mills, O. B. Toon, G. E. Thomas, Mesospheric sulfate aerosol layer, Journal of Geophysical Research: Atmospheres 110 (2005).

27. C. George, et al., Emerging areas in atmospheric photochemistry, Atmospheric and aerosol chemistry pp. 1–53 (2012).

28. C. von Savigny, et al., The research unit volimpact: Revisiting the volcanic impact on atmosphere and climate–preparations for the next big volcanic eruption, Meteorologische Zeitschrift pp. 3–18 (2020).

29. C. Bertolin, F. Domınguez-Castro, The earliest datable noctilucent cloud observation (parma, italy, ad 1840), The Holocene 30, 682–690 (2020).

30. M. Raspaud, et al., Pytroll: An open-source, community-driven python framework to process earth observation satellite data, Bulletin of the American Meteorological Society 99, 1329–1336 (2018).

31. L. Lastilla, V. Belloni, R. Ravanelli, M. Crespi, Dsm generation from single and cross-sensor multi-view satellite images using the new agisoft metashape: The case studies oftrento and matera (italy), Remote Sensing 13, 593 (2021)

32. T. J. Schmit, et al., A closer look at the ABI on the GOES-R series, Bulletin of the American Meteorological Society 98, 681–698 (2017).

33. K. Bessho, et al., An introduction to himawari-8/9—japan's new-generation geostationary meteorological satellites, Journal of the Meteorological Society of Japan. Ser. II94, 151–183 (2016).

34. D. Kim, M. Gu, T.-H. Oh, E.-K. Kim, H.-J. Yang, Introduction of the advanced meteorological imager of geo-kompsat-2a: In-orbit tests and performance validation, Remote Sensing 13, 1303 (2021).

Acknowledgments

Data Availability: GOES-16 and Himawari-8 satellite data are available through NOAA's big data program: https://www.noaa.gov/organization/information-technology/list-of-big-dataprogram-datasets

GK-2A data is available via KMA's open data API: https://datasvc.nmsc.kma.go.kr/

ECMWF and GFS profile data (filename TProfs.csv) and the Python code used to perform this analysis is available on GitHub: https://github.com/simonrp84/Tonga_Volcano_Code

The lists of points used for tri- and dual-satellite parallax calculations are also on the same GitHub page (filenames: Points_Dual.csv and Points_Tri.csv). The IR and stereoscopic retrieval outputs are in the Height_Out and Heightmap subdirectories respectively.

Supplementary Materials
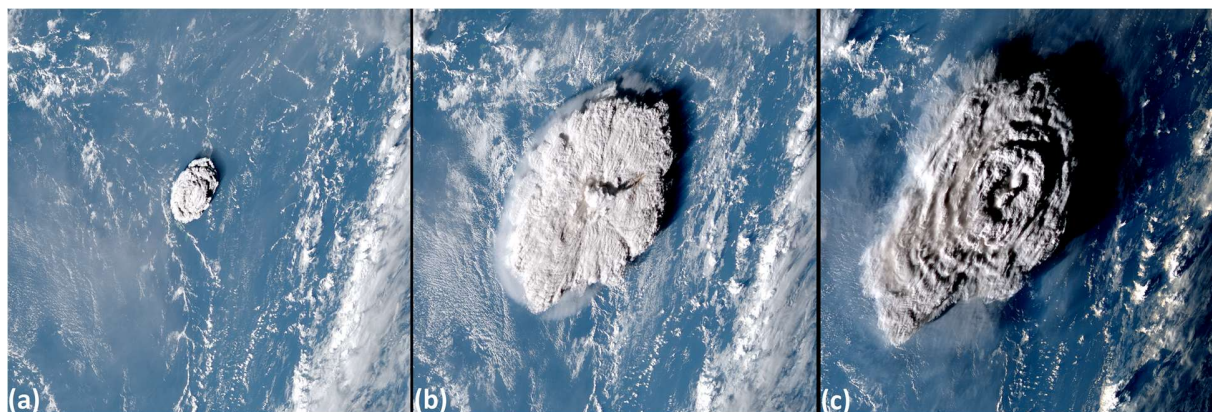
Materials and Methods

Table S1

Fig. 1. The Hunga-Tonga eruption viewed from the Himawari-8 weather satellite. (a) At 04:10 UTC, approximately ten minutes after the Eruption began. (b) At 04:50 UTC after the initial dome collapsed, leaving remnants at 55-58km altitude that case a shadow (to right) onto the umbrella cloud at 34km. (c) At 05:40 UTC as the volcanic umbrella spreads South-Westwards and the sun begins to set, emphasizing the shadows that we used to calculate plume altitude and highlighting wave structure in the umbrella top.
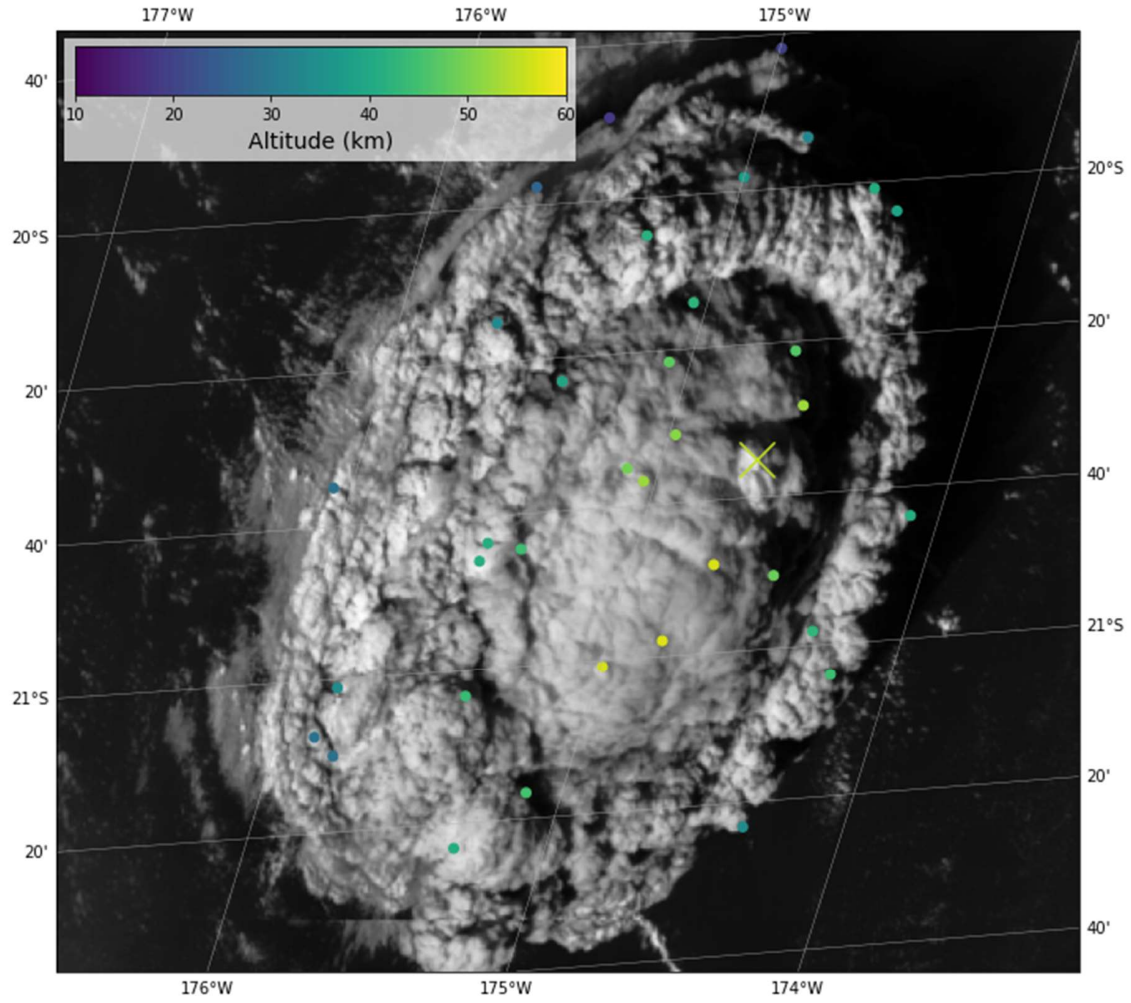
5

Fig 2. Parallax-based retrievals of plume cloud altitude at 04:30 UTC overlaid on Himawari-8 / AHI high resolution data for the same time frame. Coloured circles represent AHI-AMI retrievals and the two crosses denote AHI-AMI-ABI retrievals.
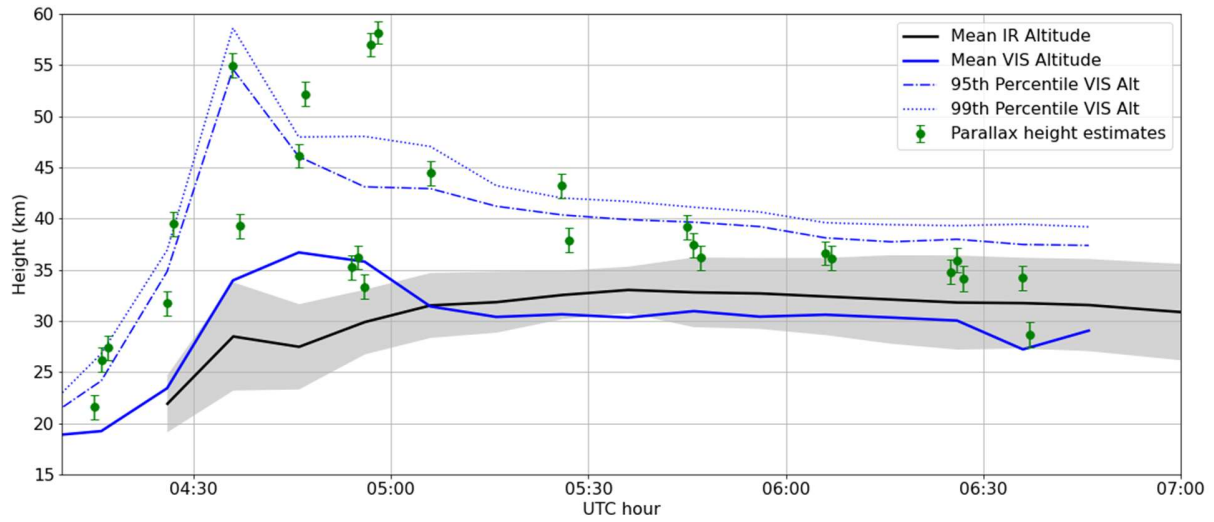
Fig 3. Temporal evolution of volcanic plume altitude derived from visible and infrared data. Infrared heights are derived from Himawari-8 brightness temperature measurements and the ECMWF temperature profile. The grey shaded area represents one standard deviation from the mean. The blue lines denote altitudes estimated via the stereoscopic method across the entire volcanic plume and the green markers are parallax heights derived from manual analysis of data from Himawari-8, GK-2A and GOES-17. Error bars show the spread of estimated altitudes due to simulated geo-location uncertainty. Due to sunset, no visible altitudes are available after 06:46 UTC.
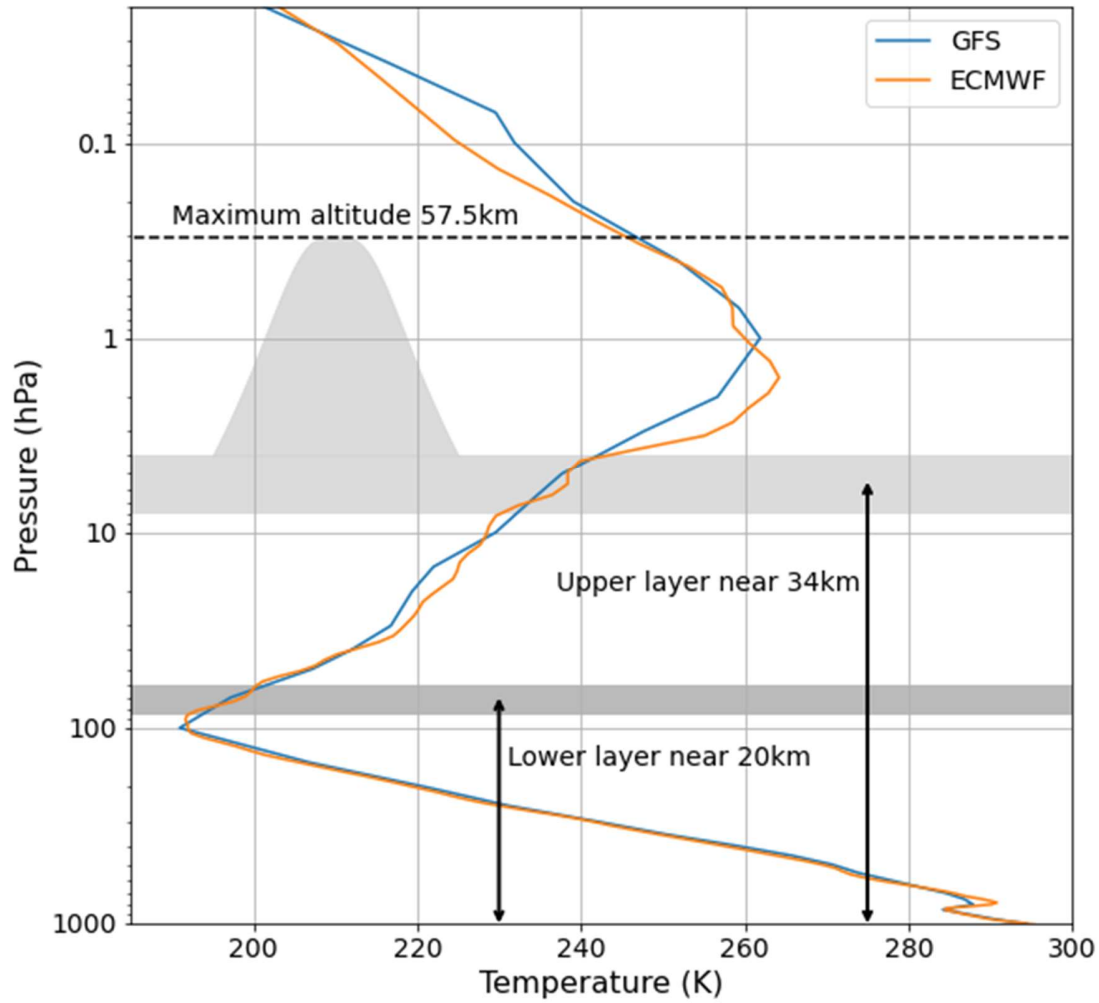
Fig 4. Vertical structure of the volcanic plume. A lower near-tropopause layer, whose altitude cannot be accurately determined, the main umbrella at higher altitude and the dome-like protrusion seen in the 04:30 UTC satellite images. Layer thickness is computed from the spread of parallax-based altitude retrievals for each layer and - when optically thick - the infrared brightness temperature approach. Overlaid are the 00:00 UTC GFS and ECMWF temperature profiles that show the tropopause near 100hPa and the stratopause at between 1-1.5hPa.